NJC

ROYAL SOCIETY OF CHEMISTRY

PAPER

View Article Online
View Journal

Cite this: DOI: 10.1039/d3nj04090a

Photocatalysis enhancement and Cl^- boosting mechanisms of peracetic acid-based advanced oxidation processes for antibiotic removal by using HOF-Cu-g-C_3N_4

Xijiang Chang,[a] Haoyu Zhang,[a] Xiaoling Liu,[b] Wenxin Li,[c] Shifei Kang,[c] Di Sun*[d] and Zilan Xiong*[e]

In recent years, the utilization of the peracetic acid (PAA)-based advanced oxidation process (AOP) for water treatment has gained significant attention. This is due to its ability to generate highly reactive species such as hydroxyl radicals (•OH) and organic oxygen radicals (R-O•), which efficiently degrade organic pollutants in water. However, traditional activation methods involving ultraviolet radiation, heat, and transition metal ions have limitations in terms of efficiency, control, and potential metal sludge production. To address these challenges, a novel heterogeneous PAA-based AOP process utilizing the HOF-Cu-g-C_3N_4 catalyst was developed for high-performance antibiotic removal. This approach effectively coordinates the reaction interfaces, activation sites, and light energy harvesting for enhanced activity and sustainability. X-ray photoelectron spectroscopy (XPS) analysis of HOF-Cu-g-C_3N_4 indicated that heterogeneous catalysis occurred at two different active sites on the catalyst's surface. The analysis also revealed that the presence of hydroxyl radicals (•OH) and organic radicals (such as $CH_3C(O)O$• and $CH_3C(O)OO$•) played a significant role in the generation of free radicals in the PAA system. These free radicals were found to dominate the oxidative degradation of antibiotics. The degradation of antibiotics was observed to be effective over a wide pH range, especially at near-neutral pH. Interestingly, the addition of Cl^- ions was found to have a notable promotion effect on the degradation of antibiotics. The electrochemical characterization results and free radical measurement provided evidence for the most plausible free radical mechanism and the Cl^- ion boosting mechanism. These findings highlight the environmental applicability and versatility of the HOF-Cu-g-C_3N_4 catalyst for the advanced treatment of refractory pollutants.

Received 1st September 2023,
Accepted 17th November 2023

DOI: 10.1039/d3nj04090a

rsc.li/njc

1. Introduction

Advanced oxidation technologies, represented by the Fenton method, have been widely employed for wastewater treatment in various industries including pesticides, dyes, cosmetics, and pharmaceuticals, owing to their exceptional performance. However, these methods also possess certain drawbacks, such as the requirement for precise pH conditions, generation of hazardous waste from iron sludge, and complicated catalyst recovery processes. Despite the development of effective strategies, such as heterogeneous Fenton systems to enhance pH adaptability and the introduction of combination technologies like photo-Fenton and electric-Fenton to enhance iron cycling, several challenges persist. These include the limited presence of free radical species and the short lifespan of hydroxyl radicals. Consequently, it is essential to explore new advanced oxidation systems that incorporate multiple free radical species and exhibit improved adjustability.[1]

In recent years, the catalyst activated peracetic acid (PAA) system has emerged as a prominent advanced oxidation system. PAA possesses a molecular structure with an intramolecular hydrogen bond between carbonyl oxygen and hydroxyl hydrogen. It exhibits low boiling point (110 °C), low melting point (0.2 °C), and a high dissociation constant

[a] College of Science, Donghua University, 201620, Shanghai, China. E-mail: changxj@dhu.edu.cn
[b] China Electronics Technology Group Corporation 2nd Research Institute, 030024, Taiyuan, China
[c] Department of Environmental Science and Engineering, University of Shanghai for Science and Technology, 200093, Shanghai, China
[d] Department of Ultrasound in Medicine, Shanghai Jiao Tong University Affiliated Sixth People's Hospital & Shanghai Institute of Ultrasound in Medicine, 200233, Shanghai, China. E-mail: disun@shsmu.edu.cn
[e] State Key Laboratory of Advanced Electromagnetic Technology, Huazhong University of Science and Technology, 430074, Wuhan, China. E-mail: zilanxiong@hust.edu.cn

(pK_a = 8.2). Additionally, PAA's oxidation–reduction potential ranges between 1.06 and 1.96 V, making it stronger than H_2O_2 (1.78 V), Cl_2 (1.48 V), ClO_2 (1.28 V), and Fe(VI) (0.9–1.9 V). Consequently, PAA finds widespread application as a disinfectant in food processing, medical care, and textile industries. The strong polar O–O bonds in PAA are easily breakable, leading to the production of diverse active radicals,[2] including $^{\bullet}OH$, methyl ($CH_3^{\bullet}$), alkoxy ($R–O^{\bullet}$), acetoxy group ($CH_3COO^{\bullet}$), and acetylperoxy ($CH_3C(O)OO^{\bullet}$). Moreover, PAA's peroxide bond energy (159 kJ mol^{-1}) is weaker than that of H_2O_2 (213 kJ mol^{-1}), potentially resulting in higher efficiency.[3] Consequently, utilizing PAA for the advanced oxidation process (AOP) for pollutant degradation is highly reasonable and feasible. To achieve controlled generation of variable free radicals, it is commonly necessary to incorporate catalysts such as transition metal oxides or carbon nanotubes, or employ energy excitation methods like light or heat. Among these, the activation of metal ions has proven most effective. However, the efficiency and controllability of traditional methods have not been effectively aligned.[4,5] Similar to the Fenton system, using iron-containing materials as catalysts still presents challenges including ineffective reduction and ferrikinetics of trivalent iron, resulting in the enrichment, hydrolysis, and precipitation of Fe(III), ultimately leading to the formation of hazardous iron sludge waste.[6] Consequently, the development of a controllable PAA advanced oxidation system remains highly challenging.

In order to enhance the PAA advanced oxidation process, three effective approaches have been identified.[7,8] Firstly, the substitution of Fe and Co with Cu as the catalyst offers advantages such as higher catalytic activity and lower required ion concentration, reducing the likelihood of metal sludge formation. Secondly, incorporating photocatalytic materials alongside transition metals as catalysts, following the principle of photo-Fenton systems used in conventional heterogeneous Fenton-like systems, can significantly improve the overall sustainability of the catalytic system. The introduction of photogenerated electrons, generated through photocatalysis, enhances the reduction and re-usability of high-valent metal ions. Thirdly, the incorporation of porous and mesoporous materials further optimizes the reaction interface and enhances mass transfer, leading to improved reaction efficiency. However, the integration of these three improvement strategies is currently limited, and there are rare reports of successful collaboration thus far. During our early development of a high-quality photo-Fenton catalyst, porous Fe/Cu-g-C_3N_4 was discovered. Due to good energy flow and free radical generation, it holds promising potential as a catalyst in the development of high-quality PAA advanced oxidation systems.[9–11] In this study, copper(II) nitrate was used as the copper source to synthesize a hydrogen bonded organic framework (HOF) precursor through a hydrothermal reaction with melamine and nicotinic acid. The HOF precursor was then subjected to a thermal polymerization process to incorporate carbon nitride, resulting in the formation of HOF structure carbon nitride (HOF-CN). The copper source was further combined with carbon nitride using the hydrothermal method, and the resulting mixture was dried at 100 °C to synthesize the HOF structure containing the copper carbon nitride (HOF-Cu-CN) catalyst. Based on comprehensive characterization of the physicochemical and photoelectric properties of the HOF-Cu-CN catalyst, we proceeded with advanced oxidation applications of peroxyacetic acid (PAA). It was determined that the HOF-Cu-CN-B catalyst exhibited excellent suitability for advanced oxidation systems of peracetic acid (PAA) with appropriate active site modulation. To further enhance the efficiency of the advanced oxidation process utilizing peroxyacetic acid (PAA), in this work we were astoundingly pleased to discover that the introduction of chloride ions remarkably amplifies both the proficiency in free radical generation and the rate of degradation. The mechanism behind the superior catalytic activity of the HOF-Cu-CN-B catalyst in PAA systems under high chlorine environments was thereby investigated, as well as the catalyst's reusability performance.

2. Experimental section

2.1. Preparation of graphitic carbon nitride (g-CN)

Raw graphitic carbon nitride (g-C_3N_4) control was synthesized by direct thermal polymerization of Melamine in a covered ceramic crucible at 550 °C for 4 h. The obtained g-C_3N_4 powder have a bright yellow color after natural cooling to room temperature.

2.2. Preparation of g-C_3N_4 catalysts with HOF structure (HOF-CN)

Similar to the previous experimental steps, 1.2 g of melamine and 0.4 g of niacin were accurately weighed and mixed with 80 mL of pure water. The mixture was then stirred for 1 hour. Afterwards, the mixed solution was transferred to a polytetrafluoroethylene material liner and subjected to a hydrothermal reaction at 190 °C for 24 hours. The resulting mixture was then centrifuged and dried at 60 °C for 24 hours, yielding the HOF precursor.[12] Next, the HOF precursor was placed into a tube furnace and heated in a nitrogen atmosphere. The temperature was increased at the rate of 2.5 °C min^{-1} until it reached 500 °C. The sample was maintained at this temperature for 2 hours. The furnace was allowed to cool down to room temperature

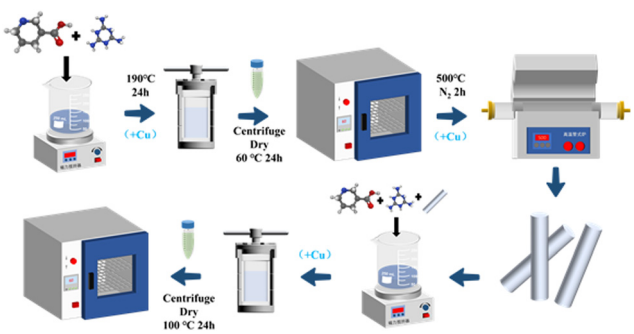

Fig. 1 Diagram showing the synthesis steps of the HOF-Cu-CN catalyst.

before removing the sample, which appeared as a light-yellow powder. This powder was denoted as the HOF-CN.

2.3. Preparation of copper-containing HOF-Cu-CN catalysts

To prepare HOF-Cu-CN catalysts, four different methods were employed depending on the step at which copper(II) nitrate was added. For record-keeping purposes, the first hydrothermal reaction is referred to as step one, calcination as step two, the second hydrothermal reaction as step three, and impregnation as step four. As shown in Fig. 1, to prepare HOF-Cu-CN-B, copper(II) nitrate is added during step two. To prepare HOF-Cu-CN-C, copper(II) nitrate is added during step three. To prepare HOF-Cu-CN-D, copper(II) nitrate is added during step four. All samples are subsequently centrifuged and dried.

2.4. Material characterization

The morphology of the materials was examined using a JEM-2100 transmission electron microscope (TEM). Nitrogen adsorption–desorption analysis was performed on an Autosorb iQ2-up model analyzer. X-ray diffraction (XRD) patterns were obtained and analyzed using a Germany Brooker D8 Advance Diffractometer, with a Cu-Kα (λ = 1.5418) radiation source. Fourier transform infrared spectroscopy (FT-IR) was conducted using a Shimadzu IRTracer 100 Fourier infrared spectrometer. The chemical states of different substances in the catalyst were determined using a US Thermo SCIENTIFIC ESCALAB 250Xi X-ray photoelectron spectrometer, allowing for the investigation of surface elemental composition and chemical valence changes before and after the reaction. Ultraviolet-visible diffuse reflectance spectroscopy (UV-vis DRS) was measured using a Japanese Shimadzu UV-3600 Plus instrument. Fluorescence spectroscopy (PL) was performed using a Hitachi F-7000 fluorescence spectrometer to analyze the photoluminescence spectrum of the sample at a wavelength of 357 nm. Electrochemical characterization was conducted using a CHI660C Apparatuses electrochemical workstation, and the separation efficiency of photo-generated carriers in the sample was analyzed through a three-electrode system. Electrochemical experiments were carried out in a 0.5 M Na_2SO_4 electrolyte solution.

2.5. PAA-based AOP performance characterization

Initially, the catalyst and model pollutant were placed in a quartz tube, allowing them to reach adsorption–desorption equilibrium in the absence of light. Subsequently, a 1% mass ratio peracetic acid solution was added to the quartz tube, and the xenon lamp light source was switched on to initiate the photocatalytic degradation experiment. A 500 W xenon lamp was utilized as the photocatalytic light source, with light at 420 nm being filtered out. To maintain a constant temperature, the circulating cooling water device was activated at the beginning of the experiment. The concentration of pollutants and the reaction performance of the catalyst were monitored using the F-7000 spectrophotometer. After a designated period, an appropriate volume of solution was extracted using a 5 mL disposable needle tube. The solution was then filtered through a polyethersulfone material needle filter (0.22 μm × 13 mm) to remove solid particles and obtain a clear liquid. The filtered solution was transferred to a 5 mL quartz colorimetric dish, and the spectrophotometer was set to a wavelength of 357 nm (tetracycline). The absorbance was measured and recorded accordingly.

3. Results and discussion

3.1. Selection of catalysts

In this section, the degradation effect of different catalysts on tetracycline, the model antibiotic pollutant, under visible light irradiation using peracetic acid as the oxidant was investigated. The performance of HOF-Cu-CN catalysts loaded with copper in different ways, namely HOF-Cu-CN-A, HOF-Cu-CN-B, HOF-Cu-CN-C, and HOF-Cu-CN-D, was explored. Fig. 2 shows the photocatalytic curves of the removal effect of tetracycline by the HOF-Cu-CN photocatalysts and the original g-CN photocatalyst under visible light irradiation. It is observed that the pure g-CN catalyst exhibits a relatively poor photocatalytic effect. On the other hand, the photocatalytic performance of HOF-Cu-CN-A, HOF-Cu-CN-B, HOF-Cu-CN-C, and HOF-Cu-CN-D catalysts shows improvement. Among these, HOF-Cu-CN-B exhibits the best effect and is capable of achieving almost complete degradation of tetracycline within 150 minutes under visible light. Therefore, HOF-Cu-CN-B was selected as the subsequent research material.

3.2. Morphology and pore structure analysis

The introduction of the HOF structure in carbon nitride materials led to a change in morphology. The SEM image of the HOF-Cu-CN-B material (Fig. 3a) exhibited a belt-shaped morphology with a length of 5–15 μm, which is similar to previously reported carbon nitride using nicotinic acid precursor.[13] Further high-resolution TEM analysis (Fig. 3b and c) revealed that HOF-Cu-CN-B had a mesoporous morphology with

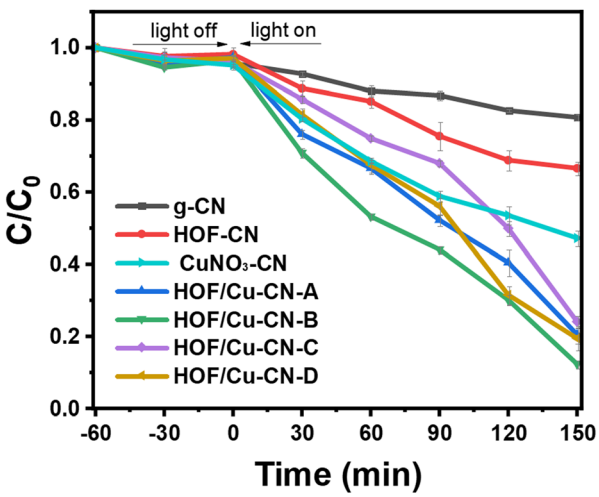

Fig. 2 Photocatalytic curves of the removal effect of tetracycline by the HOF-Cu-CN photocatalyst and the original g-CN photocatalyst under visible light irradiation.

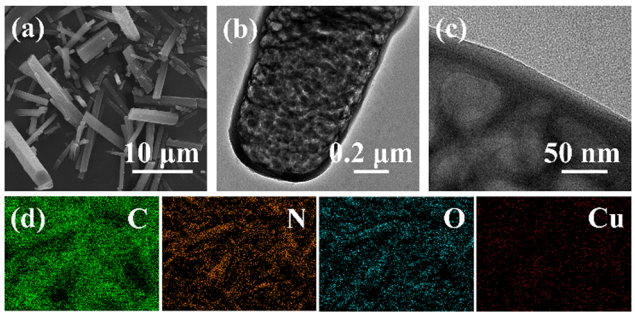

Fig. 3 (a) SEM images, (b and c) TEM images, and (d) EDS mapping images of the HOF-Cu-CN-B catalyst.

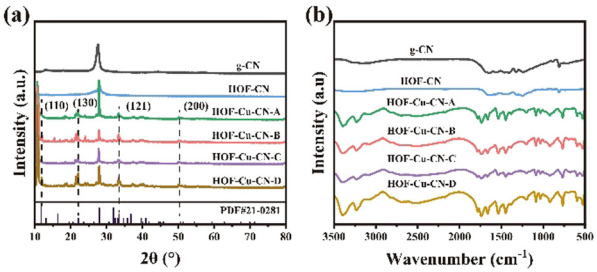

Fig. 5 (a) XRD pattern and (b) FTIR spectra of g-CN, HOF-CN and HOF-Cu-CN samples.

multiple channels inside the material, which is beneficial for electron and mass transport. The EDS mapping of HOF-Cu-CN-B confirmed the presence of carbon, nitrogen, oxygen, and copper, and all elements were evenly distributed throughout the material, as shown in Fig. 3d.

Fig. 4a presents the N_2 adsorption desorption curves of g-CN, HOF-CN, and HOF-Cu-CN-B samples. All samples exhibited H_3 hysteresis loops, indicating the presence of abundant pores in each of them. The pore size distribution curve (Fig. 4b) demonstrated that both HOF-CN and HOF-Cu-CN-B catalysts possessed smaller average pore sizes and pore volumes. While the anchoring of Cu slightly reduced the specific surface area of HOF-Cu-CN-B (19.06 $m^2\ g^{-1}$), it still remained larger than the surface area of g-CN (17.94 $m^2\ g^{-1}$). These findings indicate the favorable mesoporous properties of the HOF-Cu-CN-B catalyst, which promote the exposure of active centers in the redox reaction.

3.3. Physicochemical characterization of catalysts

In Fig. 5a, the X-ray diffraction patterns (XRD) of different catalyst materials are shown. The g-CN material exhibits characteristic diffraction peaks at 13.2° and 27.6°. The weak peak at 13.2° (100) is attributed to the stacking of aromatic structures (heptazine nitrogen units), while the strong peak at 27.6° is due to the (002) lattice plane of g-CN.[14] After modification with the HOF structure, the 13.2° peak disappears, indicating the presence of defects and porous structures embedded in the material.[15] HOF-CN shows a broad peak at 27.6 °C, indicating a smaller thickness of the synthesized material. In the various composite materials of HOF-Cu-CN, the strong peak around 10° may be due to instrument interference, while the peaks at 33.5°, 22.1°, and 11.7° correspond to the (121), (130), and (110) crystal planes of $Cu(N_3)_2$, respectively, according to the PDF #21-0281. This suggests the presence of $Cu(N_3)_2$ grains in the HOF-Cu-CN catalysts, and the peak at 50.6° corresponds to the Cu(200) crystal planes of PDF #04-0836. It should be noted that copper species may be relatively complex, and these findings imply common Cu–N bonding states, which is beneficial for understanding the catalytically active centers.

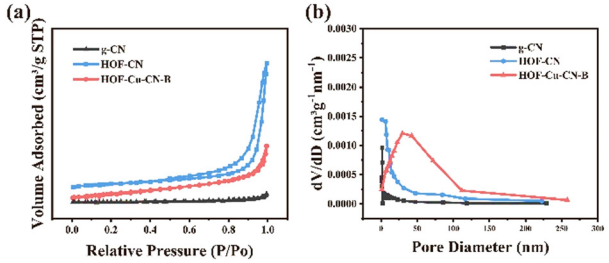

Fig. 4 (a) Nitrogen adsorption–desorption isotherms and (b) BJH pore size distributions of the as-developed g-CN, HOF-CN and HOF-Cu-CN-B samples.

Fig. 5b displays the infrared spectra of g-CN, HOF-CN, and HOF-Cu-CN. The spectra reveal the presence of characteristic vibrations of g-CN, such as signal peaks at 3240 cm^{-1} and 3390 cm^{-1} corresponding to the stretching vibrations of N–H bonds. The range of 1600–1750 cm^{-1} can be attributed to C=C bending vibrations, while the range of 1400–1550 cm^{-1} corresponds to C–H bending vibrations. The irregular tensile vibration of tris triazine rings can be observed at 1800–1100 cm^{-1}.[16] The peak at 900–1050 cm^{-1} may be associated with the deformation mode of cross-linked heptazine structures. Lastly, the characteristic peak at 807 cm^{-1} is attributed to the out-of-plane bending vibration. HOF-Cu-CN catalysts have a more abundant functional structure, which is conducive to providing a variety of adsorption and catalytically active sites.

The surface chemical states of g-CN and HOF-Cu-CN-B were characterized using XPS (X-ray photoelectron spectroscopy). In Fig. 6a, g-CN is composed of carbon (C) and nitrogen (N) elements, while HOF-Cu-CN-B also contains oxygen (O) and copper (Cu) elements except the basic C and N. Fig. 6b shows the C 1s spectra, with two main peaks observed at binding energies of 284.8 and 288.9 eV. The peak at 284.8 eV corresponds to C–C bonds (graphitic carbon), while the peak at 288.9 eV corresponds to N–C=N bonds (hybrid carbon).[17] The N 1s spectra of different materials, as shown in Fig. 6c, exhibit three main peaks: surface amino N–H_x (401.0 eV), N–(C_3) (399.7 eV), and C–N=C (398.6 eV). The presence of copper species leads to the formation of Cu–N bonds, which facilitate electron transport. In Fig. 6d, the sharp and symmetrical Cu 2p peaks at 933.1 and 952.8 eV correspond to Cu $2p_{3/2}$ and Cu $2p_{1/2}$, indicating the presence of Cu^0 or Cu^+ in the catalyst. In the triazinyl g-CN, probably Cu^+ is surrounded by triangular holes formed by three C_3N_3 rings and forms a coordinate covalent bond with the nitrogen atom on the simple aromatic ring.[18]

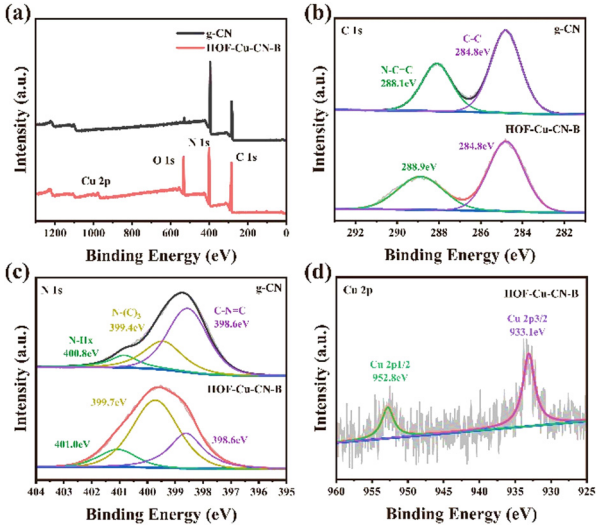

Fig. 6 (a) XPS survey spectra and (b) C 1s, (c) N 1s, (d) Cu 2p high-resolution spectra of HOF-CN and HOF-Cu-CN-B.

3.4. Electronic band structure and electrochemical analysis of the catalyst

The electronic band structure of a catalyst plays a crucial role in determining its photocatalytic and photo-AOP catalytic activity. The position of the valence band (VB) and conduction band (CB) determines the reduction potential and reducing properties of the catalyst, respectively. In the case of photocatalysts, their responsiveness to sunlight can be evaluated through their optical properties. Fig. 7a shows that all modified materials have stronger light absorption ability and wider light response range compared to pure g-CN. The absorption peak of g-CN ranges from 260 to 460 nm indicating its strong UV absorption and poor visible light response. For the optimized HOF-Cu-CN-B composite, the absorption in the visible region is greatly enlarged than that of the g-CN control, which can be contributed to the presence of Cu species and HOF porous structure. The changed UV absorption features can be ascribed to its reconstructed CN conjugate structure. This hybrid adsorption characteristic and strong visible light absorption ability make HOF-Cu-CN-B a promising photocatalyst and a photo-AOP catalyst.[19]

To estimate the optical absorption band gap energy (E_g) of the materials, the absorption spectrum is converted into the reflection spectrum using Kubelka Munk for direct band gap semiconductors. The Tauc plot intercept of $(\alpha h\nu)^2$ and $h\nu$ is then used to calculate the E_g values. For pure g-CN, HOF-CN, and HOF-Cu-CN-B, the E_g values are found to be 2.70, 2.62, and 2.58 eV, respectively (Fig. 7b). The valence band spectrum (Fig. 7c) provides information about the VB positions of g-CN, HOF-CN, and HOF-Cu-CN-B, which are found to be 2.49, 2.21, and 2.01 eV, respectively. These values are positively correlated with the oxidation potential of the photocatalyst under light irradiation and indicate its ability to generate oxidative species. Based on the data obtained from the absorption and valence band spectra, the bandgap width of the materials can be derived (Fig. 7d). The results indicate that the HOF-Cu-CN-B material has a stronger light absorption intensity and better band structure compared to pure g-CN, suggesting its superior photocatalytic and photo-AOP catalytic potential.[20]

Electrochemical impedance spectroscopy (EIS) is a technique used to evaluate the interfacial electron transfer ability of materials. By analyzing the EIS curves, the charge transfer resistance of g-CN, HOF-CN, and HOF-Cu-CN-B can be determined. Fig. 8a shows that the arc radius of the HOF-Cu-CN-B sample is much smaller than that of pure g-CN. This indicates that the HOF-Cu-CN-B composite material has a lower charge transfer resistance at the interface of the electrolyte solution, demonstrating its enhanced charge separation and transfer efficiency compared to g-CN.[21]

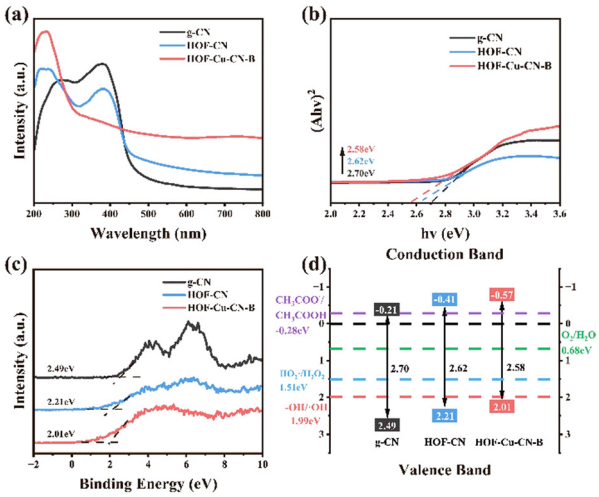

Fig. 7 (a) UV-vis DRS spectra, (b) Kubelka–Munk function curves, (c) valence-band XPS spectra, and (d) band structure of g-CN, HOF-CN and HOF-Cu-CN-B.

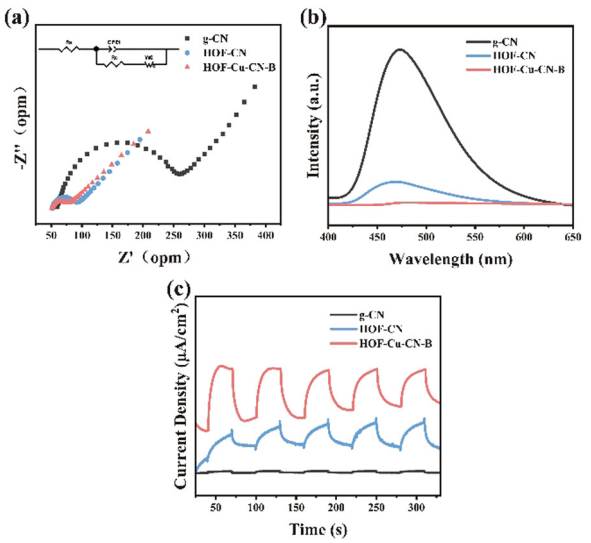

Fig. 8 (a) EIS spectra, (b) photocurrent curves, and (c) PL spectra of g-CN, HOF-CN and HOF-Cu-CN-B.

Photoluminescence spectroscopy (PL) is used to analyze the migration and recombination rates of photo-generated electron–hole pairs in the sample. Fig. 8b shows that the luminescence intensity of the HOF-Cu-CN-B composite material is significantly lower than that of pure g-CN nanosheets. This indicates that loading an appropriate amount of Cu and a hierarchical organic framework (HOF) structure helps to reduce the recombination rate of the electron–hole pairs, thus improving the photocatalytic efficiency.[22]

The transient photocurrent response of the sample under intermittent visible light irradiation was tested to investigate the migration and separation processes of the light-excited electron–hole pairs (Fig. 8c). HOF-Cu-CN-B exhibits the highest photocurrent density, indicating its efficient charge separation and transfer ability. The close contact between the Cu and HOF frameworks in the composite material effectively promotes the separation of photocharges, leading to improved catalytic activity of the photocatalyst. These results are consistent with the analysis of EIS and PL.[23]

3.5. Photocatalytic assisted advanced oxidation performance of peracetic acid

Since the removal of antibiotic compounds from aquatic environments is of high priority for human beings, antibiotics were used as model pollutants to research the effectiveness of peracetic acid (PAA) activated by the HOF-Cu-CN catalyst.[24] The degradation efficiency of tetracycline was found to reach 80–90% after 150 minutes of the reaction, while carbamazepine, sulfamethoxazole, ciprofloxacin, and norfloxacin showed degradation efficiencies of 50%, 50%, 70–80%, and 80–90%, respectively. This indicates that the system exhibited significantly enhanced photocatalytic activity, as shown in Fig. 9.

The introduction of the HOF structure and Cu species, along with the formation of Cu–N bonds, enhanced the activation

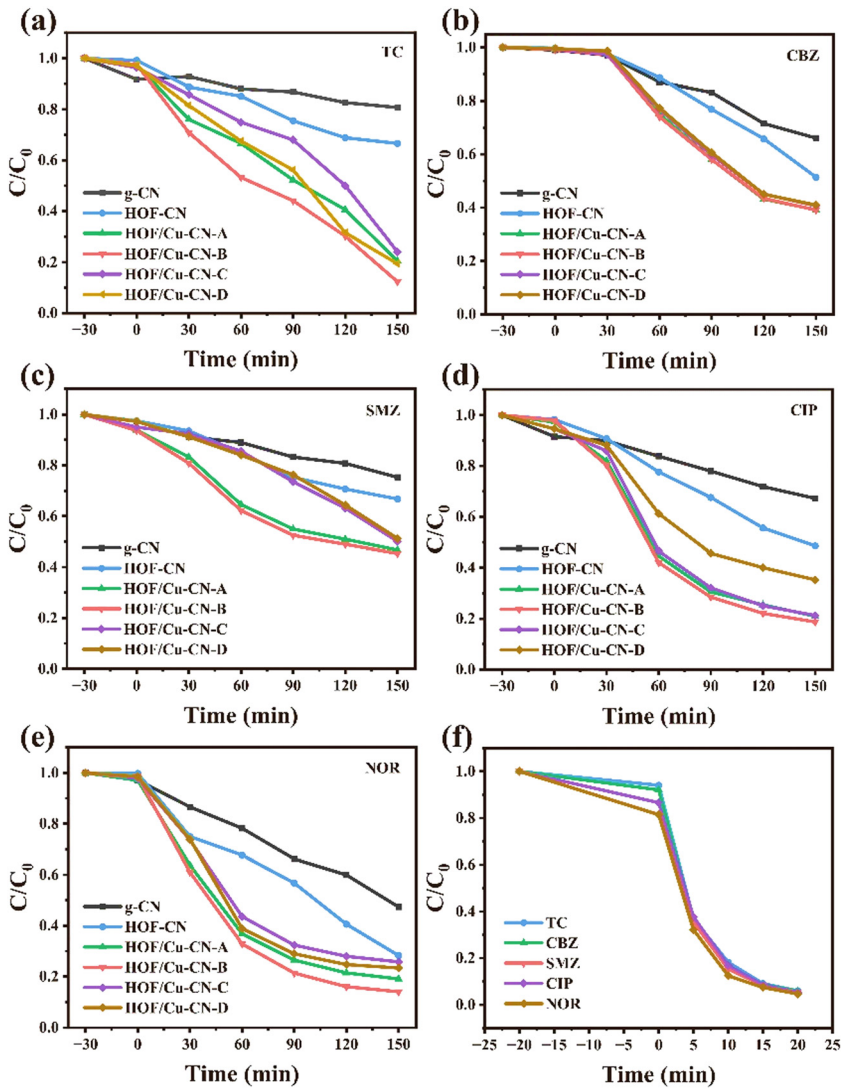

Fig. 9 Photocatalytic heterogeneous PAA-based AOP degradation efficiency of the HOF-Cu-CN-B catalyst on different contaminated substrates: (a) tetracycline, (b) carbamazepine, (c) sulfamethoxazole, (d) ciprofloxacin, and (e) norfloxacin and (f) degradation efficiency of different substrates at high chlorine concentrations of HOF-Cu-CN-B.

ability of PAA, leading to effective degradation of the antibiotics. However, the reaction rate was still slow compared with the conventional Fenton process. Further research discovered that the material could accelerate catalyst activation of PAA in high chloride environments, thereby speeding up the photocatalytic reaction rate. With HOF-Cu-CN-B as the catalyst and a Cl^- concentration of 250 mM, all five antibiotic-contaminated substrates were completely degraded within 20 minutes, significantly reducing the time required for the catalyst to degrade pollutants. This result show the great potential of using photocatalytic assisted advanced oxidation processes with peracetic acid to address the concerns of environmental pollution and potential health risks associated with their presence in water sources.

3.6. Advanced oxidation mechanisms enhanced by chloride ions

Chloride ions are widely present in wastewater as one of the most prevalent anions. Their impact on advanced oxidation systems has garnered wide attention. Negative effects stemming from chloride ion interference have been well-documented. However, recent reports have highlighted the potential promoting effect of chloride ions on the peracetic acid (PAA) system.[25] Despite this discovery, the specific pathway, applicability, and underlying mechanisms of this phenomenon remain unclear. To address this knowledge gap, we have undertaken further research in this domain, building upon our preliminary experiments.

In order to understand the influence of catalysts in high chloride environments, we conducted a series of control experiments using tetracycline as the substrate, as shown in Fig. 10. The experiments examined the effect of different factors on the photocatalytic reaction. First, the effect of the light source on the photocatalytic reaction was studied. It was found that even under dark conditions, the catalyst still exhibited good catalytic activity, although at a slower rate compared to the light reaction process. Next, the effect of different chloride ion concentrations on the catalytic reaction was investigated. The results showed that as the chloride ion concentration increased, the time taken for the catalyst to degrade tetracycline significantly decreased. For example, when the chloride ion concentration was 10 mM, only 40% of tetracycline was degraded within 20 minutes. However, when the concentration increased to 250 mM, the pollutants were completely degraded within the same time frame. When the concentration was further increased, complete degradation occurred within 10 minutes. These findings indicate that a high chloride environment can accelerate the activation of PAA by the catalyst, thereby increasing the reaction rate.

The influence of different chloride sources on the reaction was also examined. It was observed that sodium hypochlorite had no positive effect on the reaction in the environment, likely due to its interaction with PAA, causing a loss of reactivity. On the other hand, dichloromethane exhibited strong photocatalytic activity but was not suitable for degradation of pollutants in water due to its toxicity and potential for secondary pollution. Therefore, when activating PAA in a high chloride

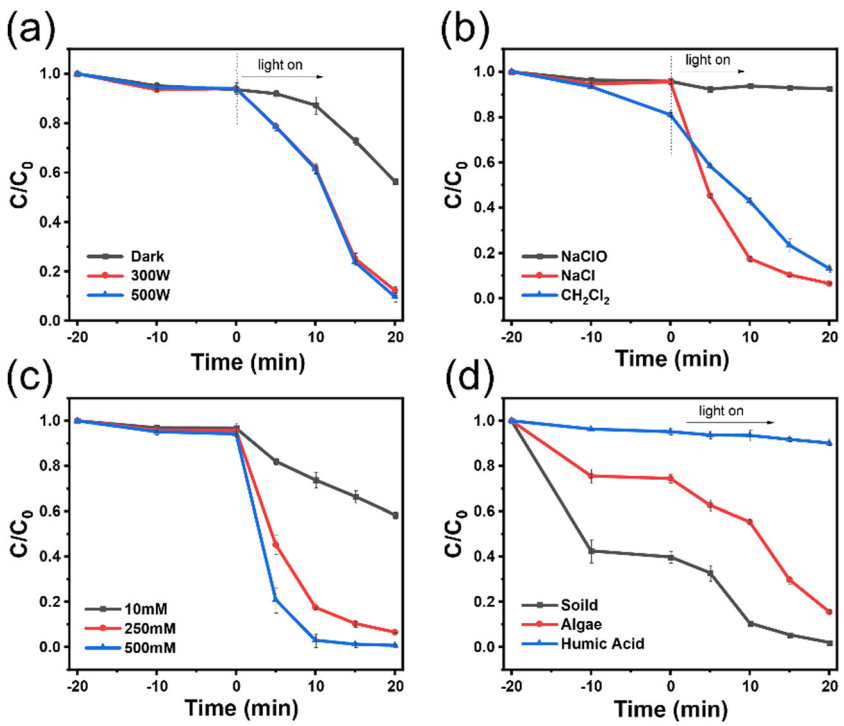

Fig. 10 Factors affecting the photocatalytic efficiency of the HOF-Cu-CN-B catalyst under a high chlorine environment, (a) xenon lamps with different watts, (b) chloride ion concentration, (c) chlorine source and (d) impurity environments.

environment, it is preferable to use NaCl instead of sodium hypochlorite or dichloromethane.

Lastly, the influence of impurities in water on photocatalytic efficiency was explored. It was found that soil and algae did not affect the efficiency of the photocatalytic reaction. However, the black color of humic acid was found to block the absorption of light by the catalyst and PAA, thereby impacting the photocatalytic efficiency. These findings remind us to pay attention to the boundaries of practical environmental applications.

3.7. Free radical mechanism and cyclic stability

The presence of active free radicals in the PAA activation process by the HOF-Cu-CN-B catalyst can be determined using *in situ* electron paramagnetic resonance (EPR) spin capture experiments. The •OH and R–C• radicals are considered key reaction species in PAA based AOPs. DMPO and TEMP are used as spin trapping agents for EPR testing. The TEMO–•OH adduct indicates the generation of •OH, and the DMPOX signal suggests the reaction between DMPO and R–C• radicals. EPR testing confirms that •OH and R–C• radicals are the main active species in the heterogeneous PAA-based AOP reactions, enabling accelerated reactions through the free radical mechanism. The stability and reusability of the HOF-Cu-CN-B catalyst throughout the reaction process are crucial for practical applications. The catalyst exhibits excellent stability and reusability, with a degradation efficiency of 85% for tetracycline even after 5 cycles.

In terms of catalyst design, although the limited electron transfer in carbon nitride hinders the activation of PAA, the introduction of the HOF structure in the HOF-Cu-CN-B catalyst provides more pore structures to facilitate electron transfer.[26] Additionally, the rich surface functional groups and defects, as well as the presence of Cu–N sites in the catalyst, contribute to the activation of PAA. The possible reaction mechanism for the degradation of pollutants in the HOF-Cu-CN-B/PAA system involves the transfer of electrons from surface electron-rich sites (Cu–N) to PAA, resulting in the generation of reactive species that degrade pollutants.

Furthermore, the synergistic mechanism of Cl^- and HOF-Cu-CN-B on PAA activation is inferred. The mechanism by which chloride ions promote enhanced radical efficiency and degradation rate is still not fully understood and requires further research. In general, it is believed that the presence of chloride ions influences the redox reactions and electron transfer processes within the reaction system. Recently, the presence of HClO intermediates has received attention. In a highly significant recent study, the activation mechanism of PAA using biochar-derived dissolved black carbon were comprehensively elucidated through the utilization of *in situ* and *ex situ* techniques. Radical species (*i.e.*, •OH and $SO_4^{\bullet -}$) as well as singlet oxygen ($^1O_2$) were not the dominant contributors, while the Cl^- induced formation of hypochlorous acid (HClO) was confirmed to be the primary oxidative species responsible for BPA oxidation.[27] On the other hand, by preferentially consuming HClO, the oxidation of BPA can be inhibited. Owing to the oxidation of HClO, typical chlorinated derivatives of BPA were identified in DBC/PMS processes, revealing a high-risk potential towards aquatic organisms.

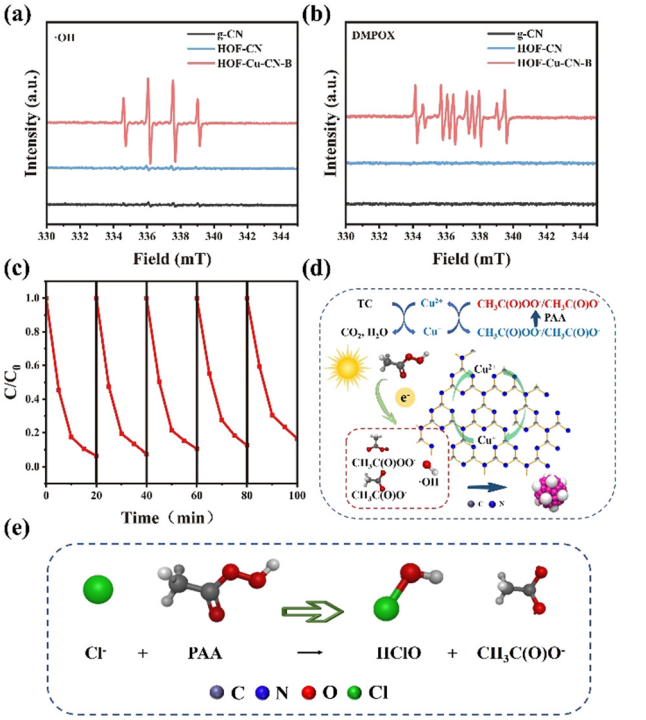

Fig. 11 EPR spectra of (a) •OH and (b) DMPOX. (c) Reusability of HOF-Cu-CN in activating PAA to degrade tetracycline (initial concentration: 20 mg L^{-1}). (d) Catalytic mechanism of the HOF-Cu-CN + PAA system and (e) schematic diagram of the conversion of Cl^- to HClO in the presence of PAA.

Based on the valuable experience and knowledge mentioned above, we propose a mechanism for this characteristic chloride ion boosted heterogeneous PAA-based AOP reaction. In our opinion, Cl^- can be oxidized by PAA to form HClO, which is adsorbed onto the catalyst surface to form a metastable HOF-Cu-CN-HClO system (Fig. 11). The strong interaction between HOF Cu CN and HClO facilitates the transfer of electrons, leading to the breaking of the Cl–O bond and the conversion of Cu^+/Cu^{2+}. This enhances the electron transfer between PAA and pollutants, improving the catalytic performance of the composite materials for pollutant degradation. The main reactions involved are as follows:

$$e^- + CH_3C(O)O^\bullet \rightarrow CH_3C(O)O^\bullet + HO^- \quad (1)$$

$$CH_3C(O)OOH + CH_3C(O)O^\bullet \rightarrow CH_3C(O)OO^\bullet + CH_3C(O)OH \quad (2)$$

$$CH_3C(O)O^\bullet \rightarrow CH_3^\bullet + CO_2 \quad (3)$$

$$CH_3^\bullet + CO_2 \rightarrow CH_3COO^\bullet \quad (4)$$

In addition, it should be noted that Cl^- is widespread in natural water, tap water and wastewater. For example, the residual chlorine in drinking water is generally in the range of 0.05–0.3 mg L^{-1} worldwide. In wastewater, there are significant differences in chloride ion content depending on

whether the treatment process involves pH regulation. Indeed, in some scenarios, the content of Cl ions in natural water is already high, and it is not necessary to add a catalyst to produce a significant PAA accelerated activation effect. Our research is committed to providing important evidence for the controllable activation of PAA in industrialization, and prompts researchers and industry to pay more attention to the interaction between chloride ions and PAA activation catalysts. In short, although the addition of catalysts may not always be necessary, understanding the technology and mechanism of initiative activating PAA by using catalysts is meaningful.

4. Conclusion

In conclusion, the HOF-Cu-CN catalyst was regulated to process appropriate active sites, thus suitable for activating the PAA-based AOP system. The morphology, microstructure, surface chemical composition, and optoelectronic properties of the HOF-Cu-CN material were characterized using TEM, SEM, FTIR, XPS, and electrochemical methods. In a high chlorine environment, the material combines with H^+ ions in the solution to generate HClO, which synergistically degrades pollutants through the generation of hydroxyl and acetyl oxygen radicals. This enhances the catalytic efficiency and overcomes the issue of slow degradation of pollutants in the PAA system. The developed HOF-Cu-CN material exhibited high photocatalytic activity in the degradation of various antibiotics (such as tetracycline, carbamazepine, sulfamethoxazole, ciprofloxacin, and norfloxacin) by activating PAA. The degradation efficiency of HOF-Cu-CN-B for tetracycline reached 90% after 150 minutes of reaction. The study also found that the degradation time of pollutants by the catalyst was significantly reduced with the increase in chloride ion concentration. The activation of PAA by the HOF-Cu-CN-B material resulted in more than a 6-fold increase in the photocatalytic reaction rate, and the degradation efficiency remained at 85% after 5 reaction cycles. Additionally, the effects of different light sources, chloride ion concentration, chloride-containing compounds, and impurities on PAA activation by the HOF-Cu-CN material for antibiotic degradation were analyzed in a high chlorine environment. This study has discovered an efficient photocatalysis enhanced PAA-based AOP system and provided new ideas and insights into the PAA-based AOP technology boosted by active chlorine species. The findings of this study have profound implications for future scientific research and engineering applications of advanced oxidation processes using PAA in both environmental and medical contexts.

Author contributions

Conceptualization: X. C. and Z. X.; methodology: D. S.; formal analysis: X. L. and H. Z.; investigation: W. L. and S. K.; resources: D. S.; data curation: H. Z. and W. L.; writing—original draft preparation: X. C. and S. K.; writing—review and editing: D. S. and Z. X.; supervision: Z. X.; funding acquisition: X. C. All authors have read and agreed to the published version of the manuscript.

Conflicts of interest

There are no conflicts to declare.

Acknowledgements

This research was funded by the National Natural Science Foundation of China, grant number 12175035 and 82171954.

Notes and references

1 R. Li, D. Speed, D. Siriwardena, S. Fernando, S. M. Thagard and T. M. Holsen, Comparison of hydrogen peroxide-based advanced oxidation processes for the treatment of azole-containing industrial wastewater, *Chem. Eng. J.*, 2021, **425**, 131785.

2 T. Zhang and C. H. Huang, Modeling the Kinetics of UV/Peracetic Acid Advanced Oxidation Process, *Environ. Sci. Technol.*, 2020, **54**, 7579–7590.

3 C. Shi, C. Li, Y. Wang, J. Guo, S. Barry, Y. Zhang and N. Marmier, Review of Advanced Oxidation Processes Based on Peracetic Acid for Organic Pollutants, *Water*, 2022, **14**, 1–20.

4 G. Zhou, R. Zhou, Y. Liu, L. Zhang, L. Zhang and Y. Fu, Efficient degradation of sulfamethoxazole using peracetic acid activated by zero-valent cobalt, *J. Environ. Chem. Eng.*, 2022, **10**, 107783.

5 L. Meng, J. Dong, J. Chen, L. Li, Q. Huang and J. Lu, Activation of peracetic acid by spinel $FeCo_2O_4$ nanoparticles for the degradation of sulfamethoxazole, *Chem. Eng. J.*, 2023, **456**, 141084.

6 Z. Xiong, H. Hu, Z. Cao, Y. Hu, D. Sun, H. Qin and S. Kang, Integration of Photo-Fenton Reaction and Membrane Filtration using Lignin@t-FeC_2O_4/g-C_3N_4 Nanofibers Toward Accelerated Fe(III)/Fe(II) Cycling and Sustainability, *Adv. Sustain. Syst.*, 2023, **7**, 1–10.

7 J. Ou, J. Deng, Z. Wang, Y. Fu and Y. Liu, Heat induced superfast diclofenac removal in Cu(II)–activated peracetic acid system: mediation from non-radical to radical pathway, *Chemosphere*, 2023, **338**, 139528.

8 T. Luukkonen and U. von Gunten, Oxidation of organic micropollutant surrogate functional groups with peracetic acid activated by aqueous Co(II), Cu(II), or Ag(I) and geopolymer-supported Co(II), *Water Res.*, 2022, **223**, 118984.

9 W. Li, C. Ding, S. Kang, W. Gao, Y. Yang and L. Cui, A Rapid Effervescent Route to Rational Activation of Cu/g-C_3N_4 and bulk MoS_2 Cocatalyst for Highly Efficient and Robust Photo-Fenton Process, *Adv. Mater. Interfaces*, 2022, **9**, 1–12.

10 C. Ding, S. Kang, W. Li, W. Gao, Z. Zhang, L. Zheng and L. Cui, Mesoporous structure and amorphous Fe-N sites regulation in Fe-g-C_3N_4 for boosted visible-light-driven

photo-Fenton reaction, *J. Colloid Interface Sci.*, 2022, **608**, 2515–2528.

11 Z. Zhang, L. Cui, Y. Wang, C. Ding, B. Sun, Z. Cao, W. Gao and S. Kang, Construction of high-performance g-C_3N_4-based photo-Fenton catalysts by ferrate-induced defect engineering, *Inorg. Chem. Front.*, 2022, **9**, 4091–4100.

12 Y. Tang, M. Yuan, B. Jiang, Y. Xiao, Y. Fu, S. Chen, Z. Deng, Q. Pan, C. Tian and H. Fu, Inorganic acid-derived hydrogen-bonded organic frameworks to form nitrogen-rich carbon nitrides for photocatalytic hydrogen evolution, *J. Mater. Chem. A*, 2017, **5**, 21979–21985.

13 Q. Li, L. Zhang, J. Liu, J. Zhou, Y. Jiao, X. Xiao, C. Zhao, Y. Zhou, S. Ye, B. Jiang and J. Liu, Porous Carbon Nitride Thin Strip: Precise Carbon Doping Regulating Delocalized π-Electron Induces Elevated Photocatalytic Hydrogen Evolution, *Small*, 2021, **17**, 2006622.

14 R. Suresh, N. S. Karthikeyan, L. Gnanasekaran, S. Rajendran and M. Soto-Moscoso, Facile synthesis of CuO/g-C_3N_4 nanolayer composites with superior catalytic reductive degradation behavior, *Chemosphere*, 2023, **315**, 137711.

15 Z. He, Z. Mo, J. Fu, P. Yan, H. Chen, Y. Song, J. Yuan, Z. Chen, H. Li and H. Xu, A bubble-assisted strategy to prepare porous ultrathin carbon nitride for highly-active photocatalytic hydrogen production, *J. Alloys Compd.*, 2022, **904**, 163788.

16 A. Chen, J. Xiao, X. Kong, L. Chen, C. Li, Y. Wei, Q. Du, W. Sun and J. Zhang, Regulating the charge density of Cu(I) single sites enriched on the surface of N3c Vacancies-engineered g-C_3N_4 for efficient Fenton-like reactions, *Sep. Purif. Technol.*, 2023, **314**, 123525.

17 X. Zhang, K. Matras-Postolek, P. Yang and S. Ping Jiang, Z-scheme WOx/Cu-g-C_3N_4 heterojunction nanoarchitectonics with promoted charge separation and transfer towards efficient full solar-spectrum photocatalysis, *J. Colloid Interface Sci.*, 2023, **636**, 646–656.

18 L. Yang, X. Ren, Y. Zhang, Z. Chen and J. Wan, One-step synthesis of a heterogeneous catalyst: Cu^+-decorated triazine-based g-C_3N_4 nanosheet formation and catalytic mechanism, *J. Environ. Chem. Eng.*, 2021, **9**, 105558.

19 Z. Cao, D. Sun, H. Hu, W. Li, Z. Xiong, M. He, S. Cai, Y. Fan, L. Zheng and S. Kang, FeC_2O_4/g-C_3N_4 self-assemble nanorods regulate stimuli-responsive ferroptosis via photo-Fenton mechanism, *Appl. Surf. Sci.*, 2023, **611**, 155671.

20 F. Li, B. Xu, X. You, G. Gao, R. Xu, X. L. Wang and Y. F. Yao, In-situ synthesis of Pd nanocrystals with exposed surface-active facets on g-C_3N_4 for photocatalytic hydrogen generation, *Int. J. Hydrogen Energy*, 2023, **48**, 12299–12308.

21 A. Habib, M. S. Khan, M. Zubair and I. U. Hasan, Ni-Doped In_2O_3 Nanoparticles and Their Composite with rGO for Efficient Degradation of Organic Pollutants in Wastewater under Visible Light Irradiation, *Int. J. Mol. Sci.*, 2023, **24**, 7950.

22 Q. Wang, N. Tuerxun, L. Xiao, Y. Wang, C. Huang and H. Du, Visible-light-driven Ni_3FeN/g-C_3N_4 Z-scheme heterostructure for remarkable photocatalytic water splitting, *J. Am. Ceram. Soc.*, 2023, **106**, 3537–3549.

23 X. Jiang, Q. Zhou and Y. Lian, Efficient Photocatalytic Degradation of Tetracycline on the $MnFe_2O_4$/BGA Composite under Visible Light, *Int. J. Mol. Sci.*, 2023, **24**, 9378.

24 M. J. F. Calvete, G. Piccirillo, C. S. Vinagreiro and M. M. Pereira, Hybrid materials for heterogeneous photocatalytic degradation of antibiotics, *Coord. Chem. Rev.*, 2019, **395**, 63–85.

25 F. Chen, L. L. Liu, J. H. Wu, X. H. Rui, J. J. Chen and Y. Yu, Single-Atom Iron Anchored Tubular g-C_3N_4 Catalysts for Ultrafast Fenton-Like Reaction: Roles of High-Valency Iron-Oxo Species and Organic Radicals, *Adv. Mater.*, 2022, **34**, 1–11.

26 D. Wang, Z. Zhang, S. Xu, Y. Guo, S. Kang and X. Chang, H_2 + CO_2 Synergistic Plasma Positioning Carboxyl Defects in g-C_3N_4 with Engineered Electronic Structure and Active Sites for Efficient Photocatalytic H_2 Evolution, *Int. J. Mol. Sci.*, 2022, **23**, 7381.

27 J. Dai, J. Yan, D. Ding and T. Cai, Dissolved black carbon induced elimination of bisphenol a by peroxymonosulfate activation through HClO mediated oxidation process, *Chem. Eng. J.*, 2022, 137179.

